

Article

Analysis of Slip Failure Characteristics and Support Deformation Law of Structural Planes and Rock Foundation Pits with Developed Karst Caves

Jin Xu  and Yansen Wang *

State Key Laboratory for Geomechanics and Deep Underground Engineering, China University of Mining and Technology, Xuzhou 221116, China; xjthm1371@163.com

* Correspondence: tb18220020b0@cumt.edu.cn

Abstract: This paper establishes a numerical analysis model for the slope of a high-inclined angle stratified foundation pit using support methods including row piles, pile-anchor supports, and combined pile-bracing-anchor supports. The reliability of the analysis conclusion was verified by comparing the stress and deformation laws of the support structures on the bedding rock side and the toppling rock side in different schemes, in conjunction with the measured data from Sanhuan South Road Station of Xuzhou Metro Line 3. In addition, on the basis of summarizing the deformation characteristics of the support structures on the bedding rock side and the toppling rock side, the design concept of sectionalized support based on the spatial effect was proposed, and the advantages of the sectionalized support design were elaborated in combination with the numerical analysis results.

Keywords: numerical simulation; rock foundation pit; supporting force; optimal design; sectionalized support control technique



Citation: Xu, J.; Wang, Y. Analysis of Slip Failure Characteristics and Support Deformation Law of Structural Planes and Rock Foundation Pits with Developed Karst Caves. *Appl. Sci.* **2022**, *12*, 4076. <https://doi.org/10.3390/app12084076>

Academic Editor: Daniel Dias

Received: 19 March 2022

Accepted: 15 April 2022

Published: 18 April 2022

Publisher's Note: MDPI stays neutral with regard to jurisdictional claims in published maps and institutional affiliations.



Copyright: © 2022 by the authors. Licensee MDPI, Basel, Switzerland. This article is an open access article distributed under the terms and conditions of the Creative Commons Attribution (CC BY) license (<https://creativecommons.org/licenses/by/4.0/>).

1. Introduction

Commonly used support methods for rock foundation pits include anchor cable retaining walls, bolting shotcretes, and pile-plate retaining walls. These methods also present some technical problems during construction in areas with complex conditions, such as excessive deformation of the local support structure, failure of anchor cable support, and excessively dense row pile spacing. These difficulties have something to do with complicated geological conditions, generally caused by potential discontinuity surfaces [1,2], which are difficult to fully detect [3].

The key to the difficulty of designing support for rock foundation pits lies in the fact that slopes with different structures have different rock types and characteristics of unfavorable geological structures; therefore, the geological properties and deformation and failure mechanisms of foundation pits are also different [4]. In most cities in Central China, the karst cave appears in the slope of urban rock foundation pit often because the engineering project is located in the Hilly area. Longitudinal and transverse faults under the bottom of foundation pit provide passage for groundwater. The layered slope is eroded by rainwater flowing down from the top of the slope for a long time, which forms the siphon phenomenon of groundwater. In other words, the surface water infiltrates from the higher terrain and discharges from the lower terrain. In the process of flow, limestone is eroded into karst caves. When excavation of foundation pit is affected by gravity, a new destructive crack is formed between karst cave and structural plane, which leads to penetration between karst caves and changes the state of sliding destruction along a single structural plane (Jin Xu, Yansen Wang. Stability analysis and the support design method of rock foundation pit with combination of structural plane and karst cave, 2022). For this rock foundation pit whose failure mode is changed by the karst cave, the support deformation characteristics have not been fully mastered at this stage. Many

scholars have analyzed the supporting methods of some typical rock foundation pits, such as Liu et al. [5], who compared the support schemes for the power transmission tower near a residential building and considered that pile-anchor support is safer than plate-rib anchor rod support, which has been demonstrated during actual monitoring. Bai et al. [6] suggested that retaining piles should be embedded into bedrock as much as possible to prevent instability of the internal support for the soil–rock composite foundation pit in the Qingdao subway using pile-anchor support. Liu et al. [7] mentioned in her study that the micro steel pipe piles used in moderately weathered and slightly weathered rock stratum with good geological properties, which have little effect on the foundation pit, can be left out and the range of steel pipe piles used was determined. Some scholars have proposed the application range of support methods such as anchor cables [8–11], anchor shotcretes [12–14] and soil nailing walls [15,16] for rock slopes. These methods are not compared in the analysis process for the suitability of the bedding rock side and the toppling rock side of the side slope with bedded rock, while the actual situation is that both sides of the bedded rock slope have their own deformation and failure characteristics [17–20], and it is difficult to obtain satisfactory support effect by adopting the same support method, which may lead to excessive deformation difference between the two sides. In addition, compared with soil slope, rock slope generally does not suffer from long and wide sliding damage, and its damage scope is usually determined by the position of vertical structural planes on both sides, which is easy to form wedge damage [21,22]. At the same time, the elastic fulcrum method is generally used for theoretical analysis of deformation of enclosure piles caused by wedge failure. Even scholars have proposed density functional theory (DFT) to calculate deformation behavior of materials [23] or to analyze changes in mechanical properties [24]. However, these methods have not solved the problem of predicting deformation of enclosure piles caused by potential discontinuities.

In conclusion, the rock foundation pit is mainly based on the design of soil foundation pit, without considering the particularity of layered rock foundation pit. This paper establishes a numerical analysis model for layered rocks by using support methods including row pile, pile-anchor support and pile-support-anchor combination, analyses the deformation regularity of pile body under traditional row pile support, and verifies the accuracy of the model by combining the measured data of foundation pit of Sanhuan South Road Station. Based on the above research results, the sectionalized support measures are innovatively proposed for rock foundation pit, which solves the problem of excessive local deformation of rock foundation pit caused by potential discontinuities in traditional support methods.

2. Analysis of the Influence of Rock Slopes of Deep Foundation Pits with Karst Caves and Structural Planes on the Failure Mode

During the simulation process, two parallel structural planes of 60° ($45^\circ + \varphi/2$) with a true spacing of 2.25 m were proposed at depths of 25 m and 20 m, as shown in Figure 1. A 3D model was adopted, with longitudinal widths of 4 m and 50 m. In addition, along the upper structural plane, a circular karst cave is set between parallel structural planes 6 m above the ground surface, and the diameter of the cave is 0.9 times the true spacing length of the structural planes to analyze the influence of the cave on the failure mode of the slope. The parameters of the rock mass and structural planes are shown in shown in Tables 1 and 2. The mechanical parameters of moderately weathered limestone in the table are taken from the middle value of the experience range in “Engineering Geology Manual” (5th edition) as the basis for model parameter assignment. Where the main slip surface has been determined, the parameters of the slip surface are based on fully weathered IV clay. Planes below the penetration line of the karst cave indicate that the rock masses cross through both structural planes, creating a penetrating failure mode between karst caves.

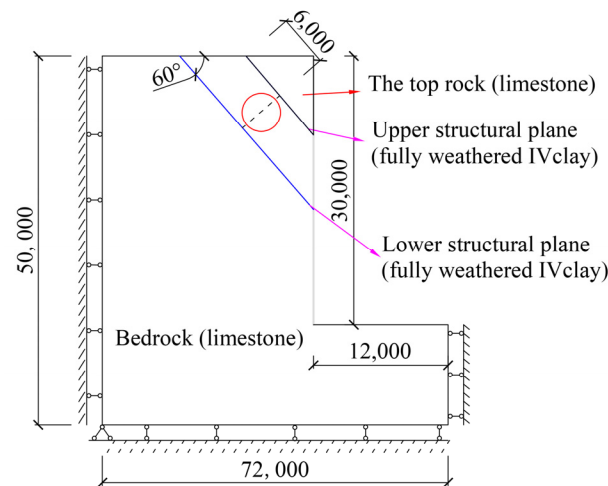


Figure 1. Schematic diagram of the numerical analysis model.

Table 1. Rock mass parameters taken as references for the stability calculation model.

Description	Density (kg/m ³)	Young's Modulus (Pa)	Poisson's Ratio	Cohesion (Pa)	Internal Friction Angle (°)	Compressive Strength (Pa)
Limestone	2300	21.0×10^9	0.22	3.0×10^6	30	1.0×10^6

Table 2. Structural plane parameters taken as references for the stability calculation model.

Description	Normal Stiffness (Pa)	Shear Stiffness (Pa)	Cohesion (Pa)	Angle of Internal Friction (°)	Compressive Strength (Pa)
Structural plane IV	2.0×10^9	1.0×10^9	2.0×10^5	15	1.0×10^5

Based on the center line of the foundation pit width, the model selects five times the excavation width of the foundation pit. The left and right boundaries of the model are constrained by the displacement in the X direction (horizontal direction), and the bottom is constrained by the displacement in the Z direction (vertical direction).

Figure 2a,b show a model with a longitudinal width of 4 m. The model uses a discount factor of 1.2 to discount the c and φ values. Figure 2 illustrates the progressive expansion of the failure from the cave to the structural plane, culminating in a broken-line failure. As shown in Figure 2b, the final failure is divided into two parts. The first part is a large triangular rock mass at the upper part of the structural plane, and the second part is the area of rock mass between the parallel structural planes below the karst cave penetration line, which indicates the rock masses crossing through both structural planes to form a penetrating failure mode between karst caves. The calculation step in the figure is to describe the deformation process of the retaining pile before the slope reaches its limit state, i.e., before the karst cave in the rock mass penetrates. The deformation results are calculated 500 times per cycle and combined into the deformation process map of the retaining pile.

For the foundation pit model with a longitudinal width of 50 m, a 3D model of the foundation pit with bedding rock and toppling rock slopes will be created to determine the failure modes and ranges of the slopes on the bedding rock side and the toppling rock side within 50 m. In the model, the positions of the karst cave and structural plane on the slope with the bedding rock structural plane are the same as those in the 4 m model; on the toppling rock side, a 60° reverse structural plane is set every 5 m along the depth direction of the foundation pit, and the structural plane and the mechanical parameters of the rock mass are the same as on the bedding rock side. On the bedding rock side, fissures with different angles are set inside the upper slip cracking rock mass to make the rock slide in

different ranges under different working conditions, while on the toppling rock side, the rock mass is completely decomposed into rock blocks with an average diameter of 0.5 m to simulate local tipping.

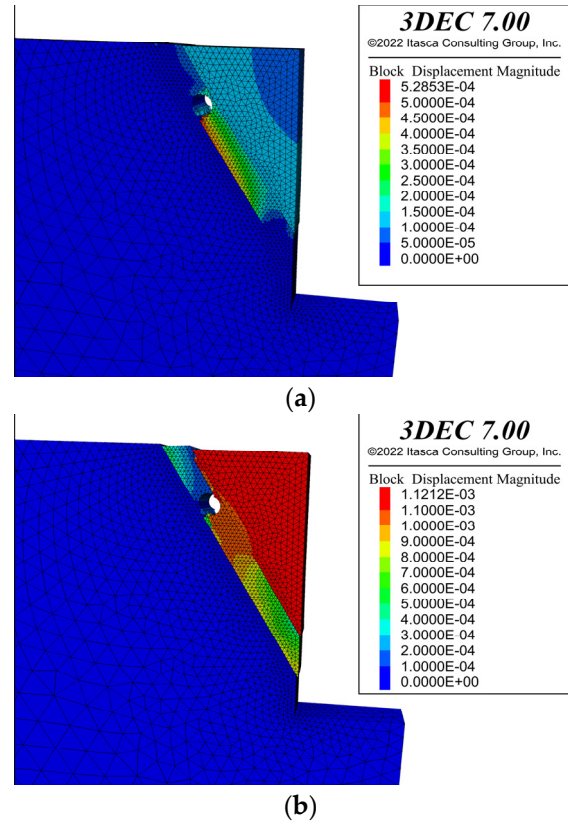


Figure 2. Failure process of a 4 m-wide rock mass with circular karst caves penetrating into the foundation pit at 60° structural plane dip angle. (a) 5000 steps; (b) 8500 steps.

As shown in Figure 3a,c, the slope on the bedding rock side forms a wedge-shaped failure area, with the entire wedge gradually sinking along the first structural plane of the penetration, while the lower part of the rock mass slides with the upper wedge, with the same failure mode as in the 4 m model. Toppling failure of the strip rock mass between the structural planes is formed on the slope at the toppling rock side, as shown in Figure 3b,c.

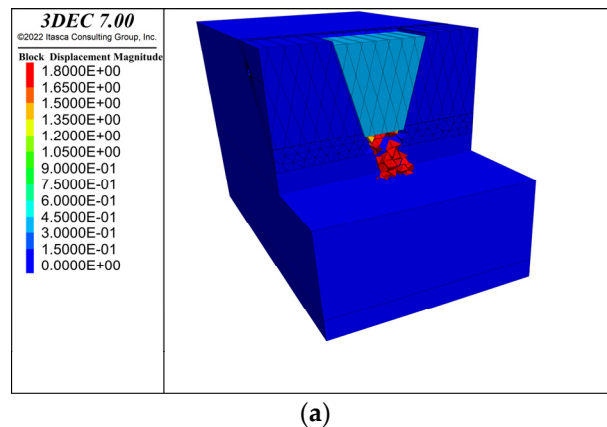


Figure 3. Cont.

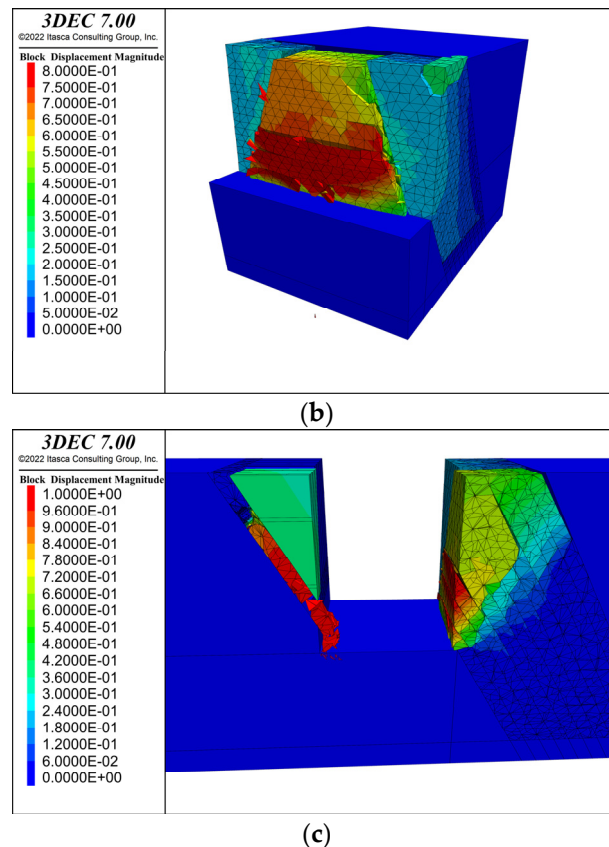


Figure 3. Cross-sectional view of failure mode of rock mass within 50 m length of foundation pit under 60° dip angle of structural plane. (a) failure mode of the foundation pit on the bedding rock side; (b) failure mode of the foundation pit on the toppling rock side; (c) section view of failure mode of the foundation pit.

Therefore, from the calculation results of the two length models mentioned above, the bedding rock side is characterized by broken line slip failure under karst cave conditions, while the toppling rock side is characterized by approximately arc-shaped toppling failure. The following support design analysis will be based on these two analysis models.

3. Numerical Simulation of Pile-Anchor Support Technology for Rock Slopes of Deep Foundation Pits

In the design and analysis of foundation pit support, it is assumed that there is a holistic penetrating failure of a single slip surface or that the breakthrough failure of a karst cave between parallel structural planes is deemed an extreme state of the foundation pit.

The row piles are set with spacings of 1.5 times, 2 times, 3 times and 4 times the pile diameter. The pile is made of C35 concrete with a length of 34 m, and the anchor cable is arranged at the maximum displacement point of the pile body. This method is widely used in Tunnel Engineering [25,26]. The length of the anchor cable is 15 m, with an anchoring section length of 7 m and an inclination angle of 15° , forming a joint pile-anchor support system in the form of one pile and one anchor.

It can be seen from Figures 4 and 5 that karst cave penetration failure still occurs after the installation of the retaining piles, which shows that the slope of the foundation pit slope supported by cantilever piles does not change the failure pattern in the cave containing condition.

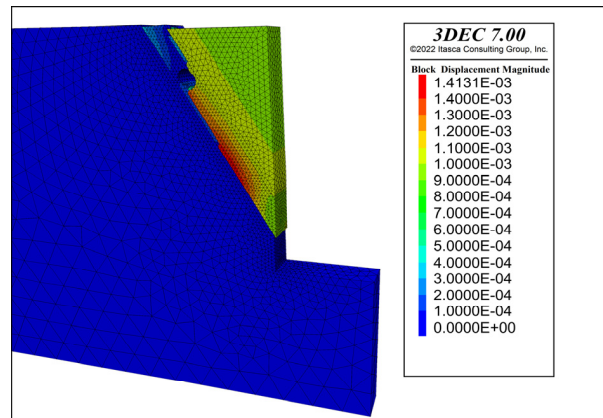


Figure 4. Pile diameter of 0.8 m, 1.5 times pile spacing, cantilever pile support (three retaining piles).

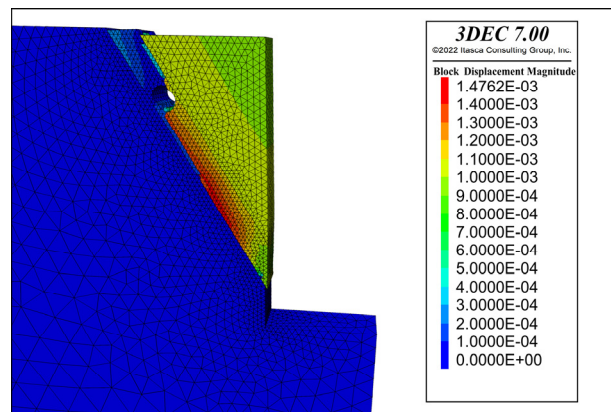


Figure 5. Pile diameter of 0.8 m, 2.0 times pile spacing, cantilever pile support (three retaining piles).

Figure 6 shows the displacement curve for a cantilever pile with a 0.8 m pile diameter and 1.5 times the pile spacing, with a maximum horizontal displacement of 0.7 mm at the ultimate condition (8000 steps). The displacement curve of the pile began to bulge slightly at 4000 steps. The position of the maximum displacement increment at the top of the pile remained unchanged, with a small displacement range until 7000 steps. After 7000 steps, the displacement increases sharply between 7000 steps and 8000 steps, with an increment in displacement twice as large as the first 7000 steps.

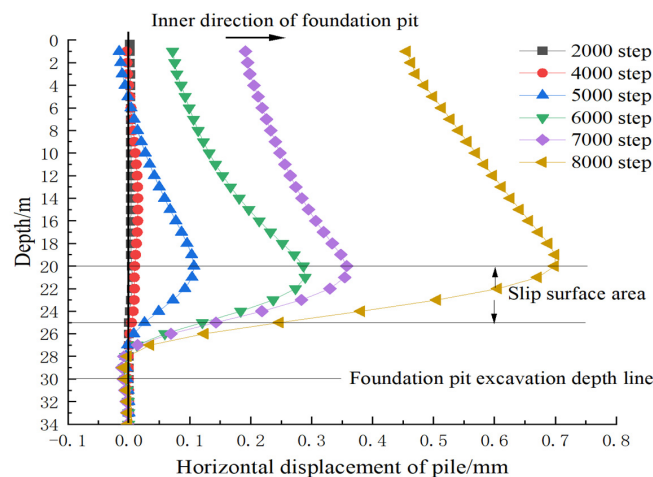


Figure 6. Displacement curve of cantilever piles with different pile diameters at 1.5 times pile spacing (three piles).

If a pile spacing of 2.0 times the pile diameter is used to support the foundation pit, the overall deformation trend of retaining piles is similar to that of the 1.5 times pile spacing case (as shown in Figure 7), and the maximum displacement values achieved at the same analysis step are consistent between the two. For the 4 m model, when the total number of retaining piles is the same, the change in pile spacing does not affect the final deformation but only slightly affects the depth of the maximum displacement point.

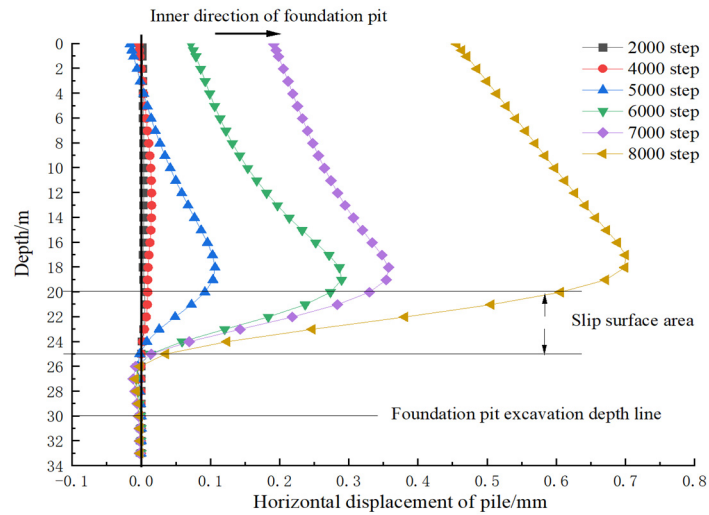
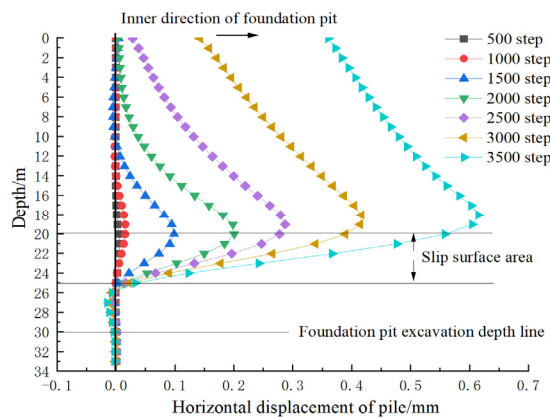


Figure 7. Displacement curve of pile body with 2.0 times pile spacing (three piles).

If the foundation pit is supported at a pile spacing of 3.0 times the pile diameter, the number of retaining piles will be reduced from 3 to 2. The extreme state is reached at 3500 steps in the calculation, as shown in Figure 8a. As shown in the working condition of the three retaining piles, there is a steep increase in the maximum displacement of the retaining piles when the foundation pit reaches extreme failure. When the crown beam is installed at the top of the retaining pile, its displacement is shown in Figure 8b. Compared with the support method without the crown beam, the occurrence time of the extreme state has shifted backward, and the displacement at the top of the retaining pile is greatly suppressed with the increase in calculation steps. After the crown beam is installed, the steep increase in pile displacement before reaching the extreme state disappears. This shows that the crown beam is necessary to avoid the collapse of the foundation pit due to the increase in instantaneous residual sliding force when the slip surface of the rock mass is penetrated.



(a)

Figure 8. Cont.

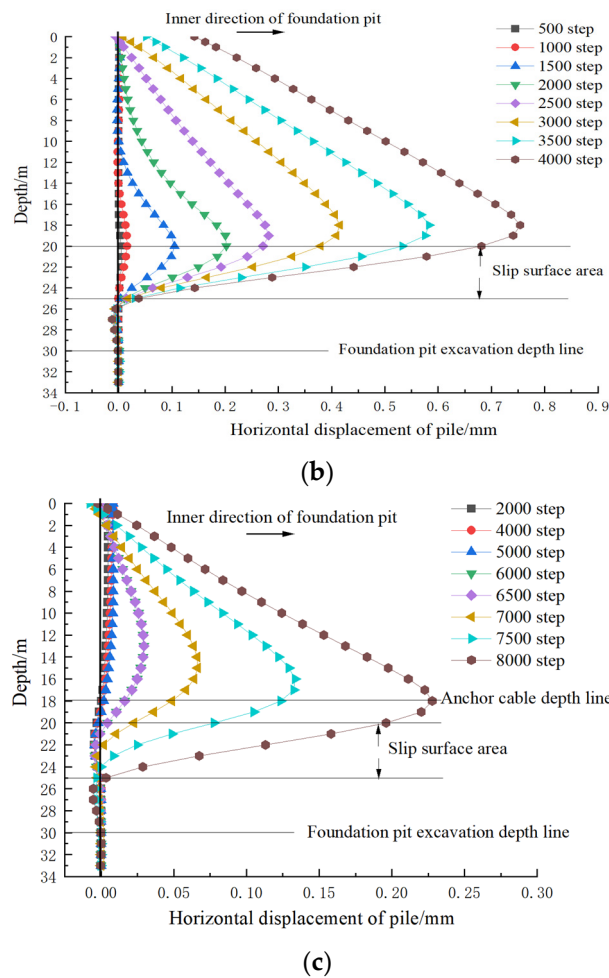


Figure 8. Displacement curve of pile body with 3.0 times pile spacing (2 piles). (a) The diameter of the cantilever pile is 0.8 m. (b) The pile diameter is 0.8 m and the crown beam is set. (c) The pile diameter is 0.8 m, and the crown beam and anchor cable are set.

In response to the maximum displacement of the retaining pile at the slip surface, under the condition that there are crown beams, two prestressed anchor cables are set in parallel at a depth of 18 m in the foundation pit, with a prestress of 300 kN applied. As shown in Figure 8c, the application of anchor cable can significantly prolong the occurrence time of the extreme state, and the maximum displacement of the pile body under the extreme state is also significantly reduced, but the maximum displacement point has changed, which appears at the application point of the anchor cable.

The pile spacing is expanded to 4.0 times the pile diameter, as shown in Figure 9. A comparison with Figure 9a shows that the final deformation of the retaining piles does not change and that the time to reach the extreme state remains unchanged after enlarging the pile diameter and keeping the total number of retaining piles constant.

When crown beams and anchor cables are applied, as shown in Figure 9b, the displacement of the pile top and pile body is greatly restrained. However, due to the influence of anchor cable spacing, the final pile displacement is greater than that under 3.0 times pile spacing. Thus, the combined pile-anchor support effect is easily affected by the anchor cable spacing, and, therefore, when anchor cable support is used, the anchor cable spacing needs to be strictly controlled.

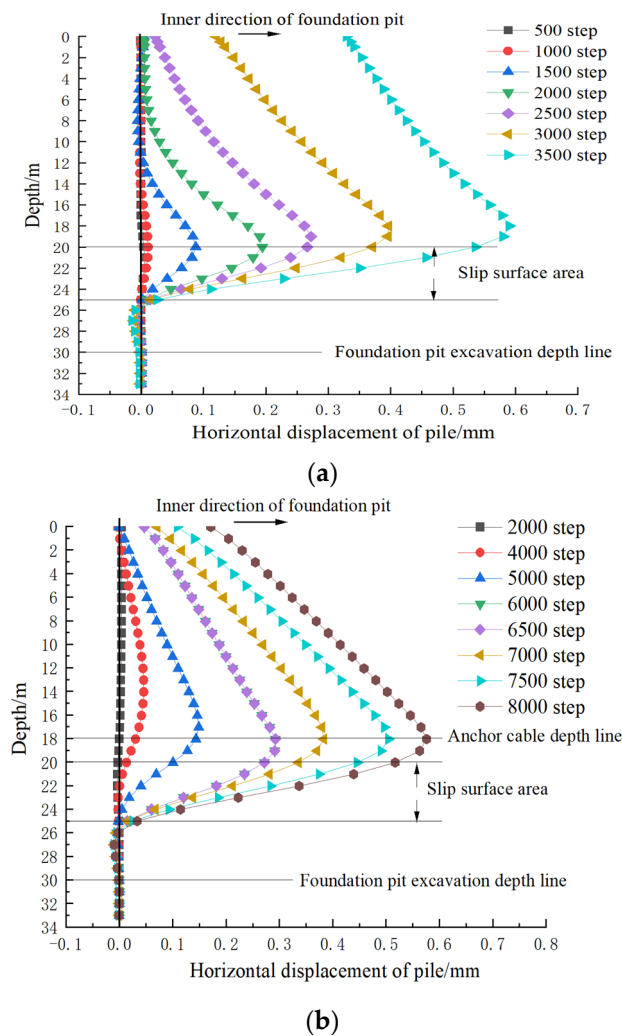


Figure 9. Displacement curve of pile body with 4.0 times pile spacing (2 piles). (a) The diameter of the cantilever pile is 0.8 m. (b) The pile diameter is 0.8 m, and the crown beam and anchor cable are set.

4. Numerical Simulation of Pile-Bracing Support Technology for Rock Slopes of Deep Rock Foundation Pits

For the model with a longitudinal length of 50 m, the following supports will be set up: concrete supports with a spacing of 7.5 m will be set at the top of the pile, with the same mechanical parameters as those of retaining piles; steel supports with a spacing of 3 m are set at 10 m of the pile body, with a support diameter of 800 mm. When the pile spacing is 1.5 times the pile diameter, the model of the foundation pit retaining pile is as shown in Figure 10a. The model, using a discount factor of 1.5, is analyzed to 12,000 steps, and the calculation results are shown in Figure 10b,c.

Figure 10b,c show the failure displacement cloud of the rock mass after supporting the bedding rock side and the toppling rock side. The slip of the slope on the left bedding rock structural plane has a greater impact on the retaining piles in the middle of the foundation pit, and the maximum impact is located in the middle and lower parts of the pile body. After the slope with the toppling rock structural plane on the right side of the foundation pit has been supported, the toppling area in the middle is well restrained. The areas with a greater influence on the pile deformation are scattered to both sides of the foundation pit. Due to the limitation of the longitudinal length of the foundation pit model, stress concentration is found at the boundary. The support of the toppling area in the middle area will be the focus of our discussion later.

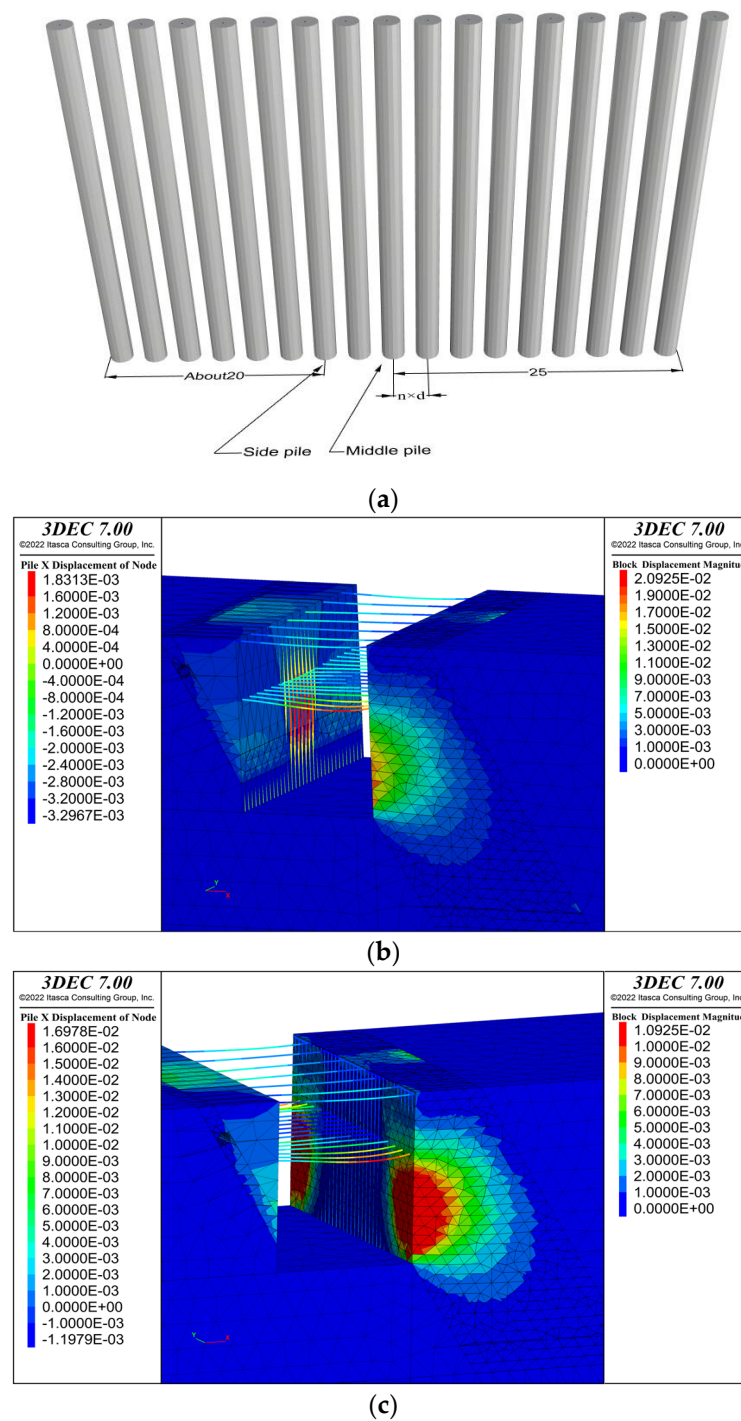
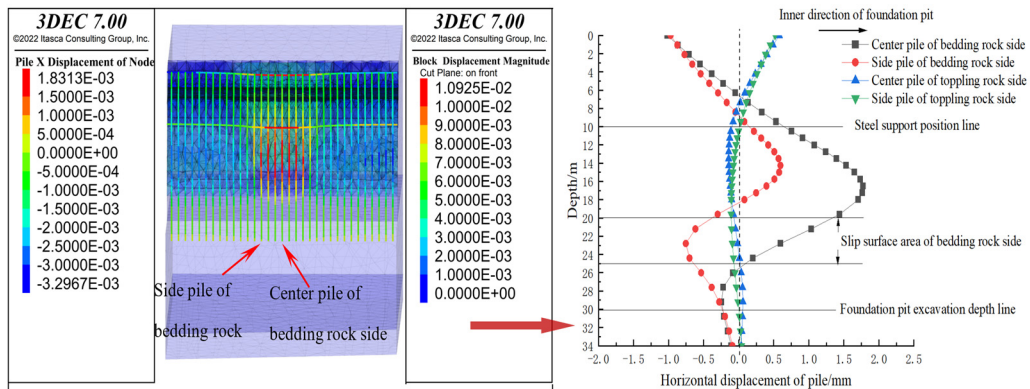


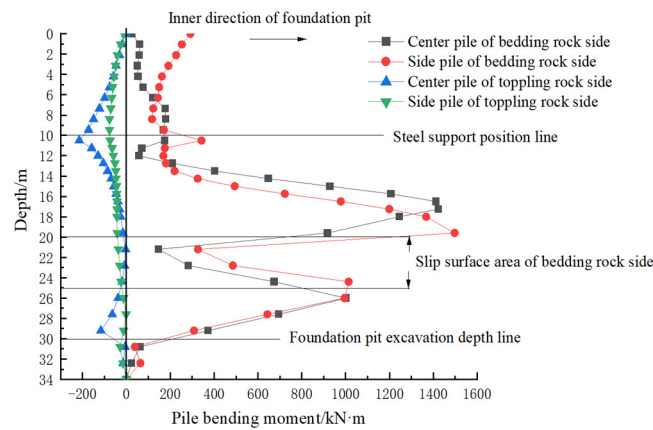
Figure 10. Numerical analysis of pile-bracing support with 1.5 times pile spacing. (a) schematic diagram for setting analysis points of retaining piles (unit: m, scale: 1:100); (b) failure and deformation cloud of bedding rock side; (c) failure and deformation cloud of toppling rock side.

Two retaining piles on the left side and right side of the model at longitudinal distances of 20 m (side pile) and 25 m (middle pile) are used for analysis, as shown in Figure 10a, hereinafter referred to as the middle pile and side pile. At the same time, the displacement and bending moment data for the crown beams and steel waist beams on the left and right sides are used to draw curve diagrams, as shown in Figures 11 and 12.



The positions of retaining piles on both sides of the foundation pit are consistent

(a)



(b)

Figure 11. Stress analysis of pile-bracing support with 1.5 times pile spacing (pile body analysis). (a) displacement diagram of the pile; (b) bending moment diagram of the pile.

The retaining pile on the bedding rock side is subjected to rock mass sliding and creates a maximum displacement in the area near the upper slip surface, resulting in a displacement toward the outside of the foundation pit. The piles below the lower slip surface slightly incline toward the rock mass, as shown in Figure 11a. The maximum deformation position of the retaining pile at the bedding rock structural plane is similar to the deformation curve of the 4 m-wide model at the structural face penetration.

The deformation of the pile on the slope with the toppling rock structural plane forms a tendency of deformation toward the inside of the foundation pit at the top of the pile, while the middle part of the piles is affected by the sliding of the bedding rock structural plane, and the stress is transmitted from the steel support to the toppling rock side, forming a slight deformation toward the rock mass. In general, the deformation of the piles on the bedding rock side slope is greater than that of the piles on the toppling rock side, and the difference in deformation between the pile and the side pile on the bedding rock side slope is significant. Due to the influence of the support structure, the sliding deformation of the rock mass in the sliding part causes the deformation of the pile structure toward the inside of the foundation pit, while the nonsliding area is also affected by the corresponding deformation but constrained by the steel support. However, the difference in deformation between the middle pile and the side pile is not significant on the toppling rock side due to the large collapse area and the dispersion of stresses.

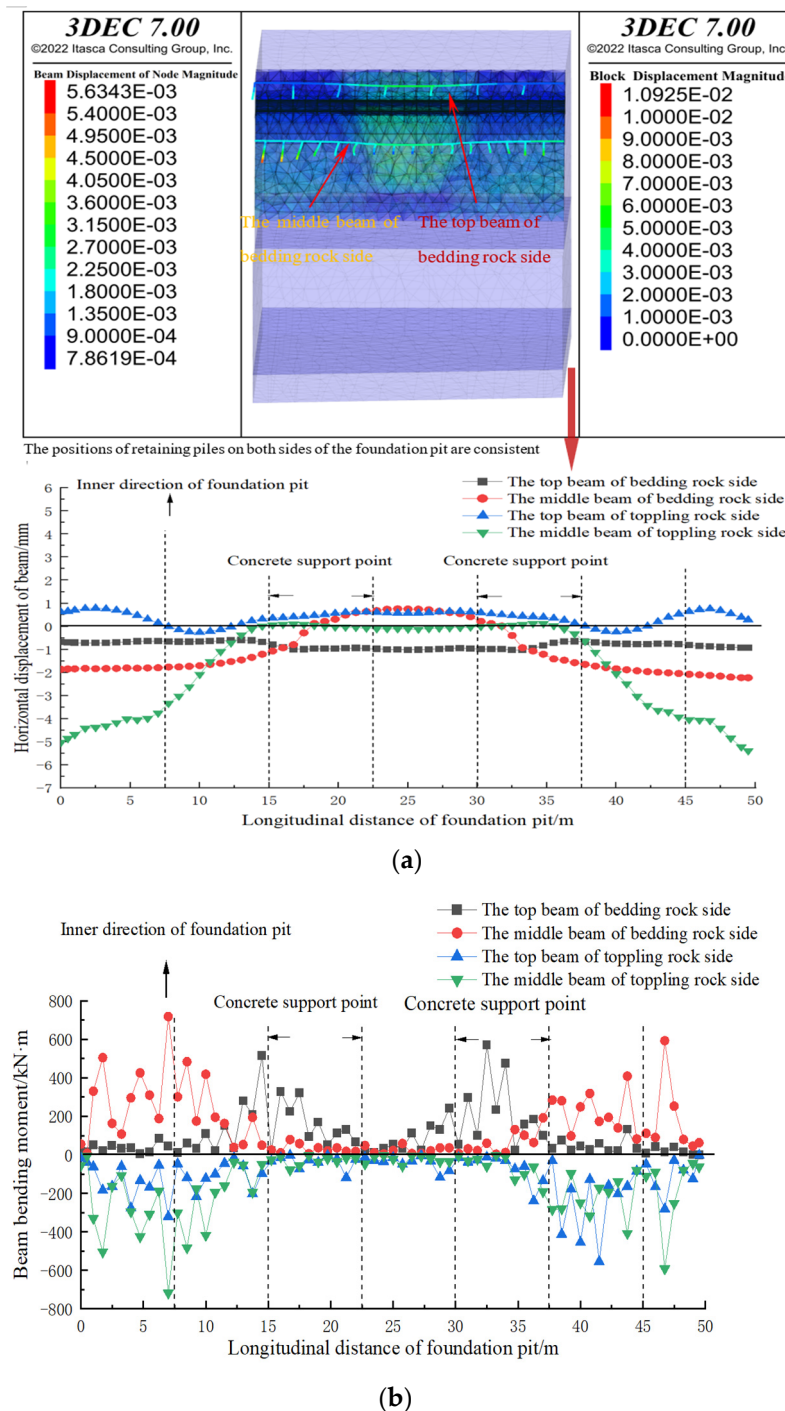


Figure 12. Analysis on the stress of pile-bracing support with 1.5 times pile spacing (analysis on the support beam). (a) displacement of support beam; (b) bending moment of support beam.

It can be seen from the bending moment diagram of the pile body that, as shown in Figure 11b, the maximum bending moment point of the pile body on the bedding rock side appears near the upper structural plane, followed by the lower structural plane, while that of the pile body on the toppling rock side appears at the steel support, followed by the excavation depth of the foundation pit. The deformation curve of the bending moment of the pile body coincides with the deformation characteristics of the rock mass.

The stress analysis curve of the crown beam and the waist beam is shown in Figure 12. From the displacement curve in Figure 12a, it can be seen that the largest deformation occurs in the middle part of the waist beam, forming bulges toward the inside of the

foundation pit. On the other hand, the crown beam on the bedding rock side moves toward the rock mass, while the middle part of the crown beam on the toppling rock side moves toward the inside of the foundation pit but with minimal displacement. The deformation and failure characteristics of the bedding rock side and the toppling rock side are consistent.

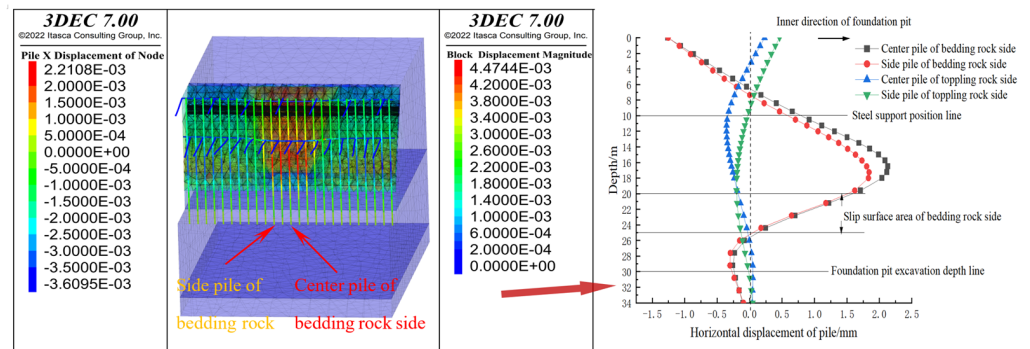
As seen from the bending moment diagrams of crown beams and waist beams, most turning points of the bending moment correspond to the supporting point on the waist beam, as shown in Figure 12b. Specifically, the maximum bending moment of the crown beams and waist beams on the bedding rock side occurs at the edges of the slip surface; the maximum moments of the crown beams and waist beams on the toppling rock side occur around the inclination surface.

5. Contrastive Analysis of Different Supporting Schemes of Rock Slopes of Deep Foundation Pits

The pile spacing on both sides of the slope is changed to 2, 3, and 4 times the pile diameter to further compare and study the effect of the pile spacing on the support effect. The pile diameter is taken as 1 m, and a discount factor of 1.5 times the pile spacing under the same conditions is adopted to calculate the extreme state to analyze the supporting effect under different pile spacings.

5.1. Supporting Analysis of the Pile Bracing Structure of the Rock Foundation Pit

For the pile-bracing support structure with a pile diameter of 2.0 times, the displacement curve is mapped out through the middle pile and the side pile, as shown in Figure 13a. The displacement change trend of the middle pile and the side pile on the bedding rock side is the same, indicating that changing deformation in the middle of the pile spacing becomes less influential on the side piles. The displacement change trend of the pile body on the toppling rock side is the same as that under a pile spacing of 1.5 times. As a whole, when the pile spacing is taken as two times the pile diameter, the maximum displacement is approximately 0.25 mm more than that of 1.5 times the pile spacing. In other words, the displacement of the pile body on the bedding rock side has increased by approximately 12.5%, while that on the toppling rock side has doubled.



The positions of retaining piles on both sides of the foundation pit are consistent

(a)

Figure 13. Cont.

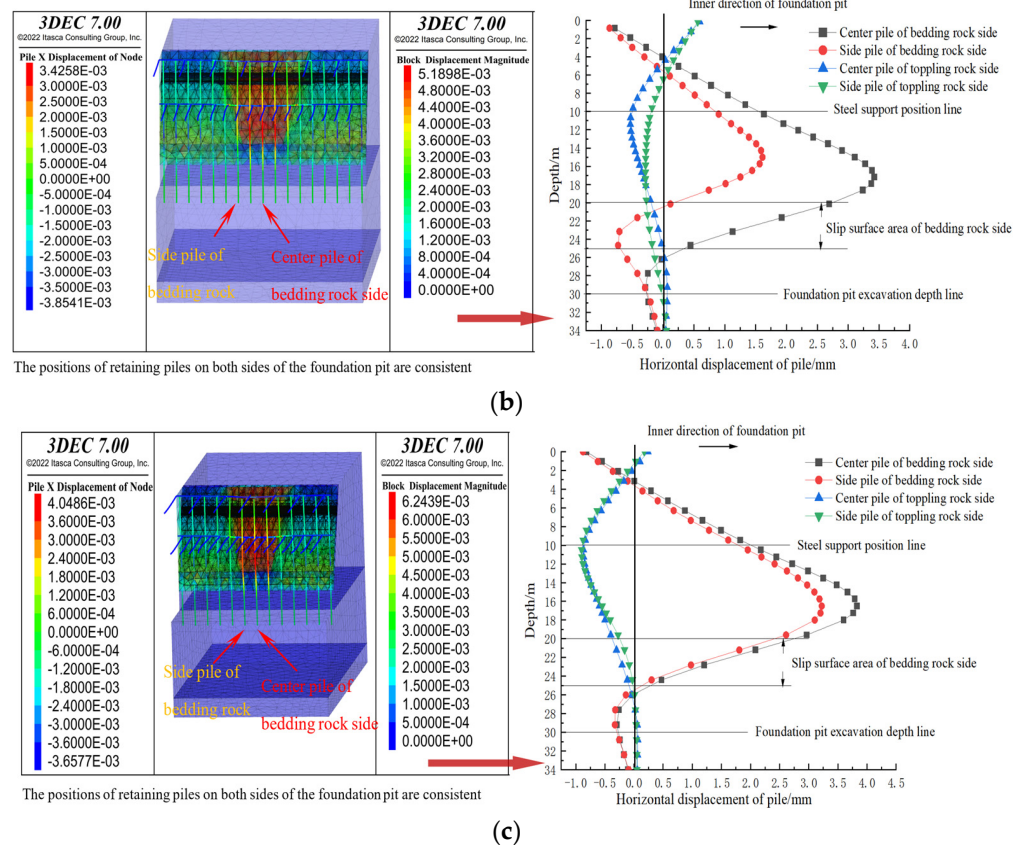


Figure 13. Analysis on the stress of pile-bracing support system. (a) displacement of retaining piles with a pile spacing of 2.0 times; (b) displacement of retaining piles with a pile spacing of 3.0 times; (c) displacement of retaining piles with a pile spacing of 4.0 times.

As seen from Figure 13b,c, the displacement of the pile body generated by 3.0 times the pile spacing and the displacement produced by 4.0 times the pile spacing are each increased. The basic rules are that the maximum displacement of the pile body is increased by approximately 1 mm when the pile spacing is increased once by the pile diameter each time; the zero point of displacement also starts moving downward; if a pile spacing of 4.0 times is reached, the deformation of the middle and side piles occurs almost simultaneously, indicating that the whole support system starts to fail. At this moment, the sliding force of the rock mass is born by the retaining pile within the range of slip. The retaining pile on the toppling rock side also faces the same conditions, and deformation on the middle piles and side piles occurs nearly synchronously when the pile spacing reaches 4.0 times.

5.2. Analysis of the Combined Support of the Pile-Bracing Anchor of the Rock Foundation Pit

The design system of the pile bracing-anchor supports is based on the 4.0 times of the pile bracing model in the previous section, with a 15 m long prestressed anchor cable set at a depth of 18 m for the bedding rock side of the retaining pile and the same length of anchor cable set at a depth of 14 m for the retaining pile on the toppling rock side to restrict the area of maximum displacement of retaining piles. The anchorage section of anchor cables is 7 m long, with an inclination angle of 15° and 300 kN prestress being applied. The layout form of “one anchor for one pile” is adopted, as shown in Figure 14a,b.

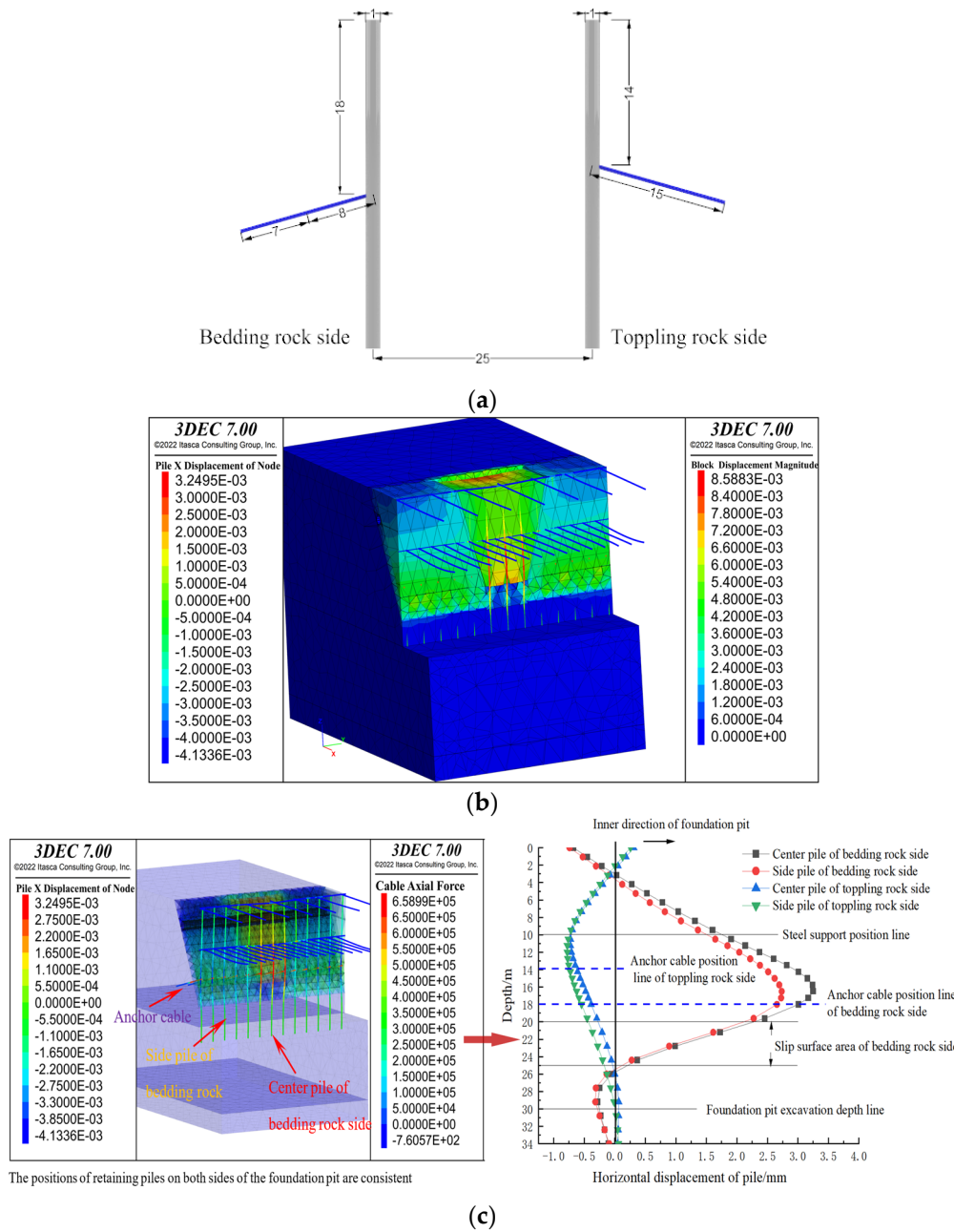


Figure 14. Analysis on the stress of combined support system of pile-bracing-anchor with 4.0 times pile spacing. (a) layout of anchor cables (unit: m); (b) displacement cloud on bedding rock side; (c) displacement of pile.

As shown in Figure 14c, when the anchor cable is applied to the 4.0 times pile spacing retaining pile, the maximum displacement value of the retaining pile on the bedding rock side decreases by approximately 12% compared to that without the anchor cable, while that of the retaining piles on the toppling rock side is decreased by only 0.2 mm. The design of the anchor cables plays no significant role in the overall safety control, considering that the pile body produces less displacement on the toppling rock side.

The rock mass on the toppling rock side is inclined toward the inside of the foundation pit. There is a supporting point on the pile body from which rotation occurs, and the anchor cable is applied with a portion of the force component generating an additional bending moment. Therefore, when anchor cables are provided for displacement control for the side slopes on the toppling rock side, the stress to the retaining piles may be increased.

According to simulation results, the anchor cables of the side slopes on the toppling rock side can be canceled.

6. Analysis Based on the Foundation Pit Project of Sanhuan South Road Station of Xuzhou Metro Line 3

Located at the intersection between the Sanhuan South Road and Beijing Road, the Third Ring Road South Station of Xuzhou Metro Line 3 has an SN layout and is a transfer station of Metro Line 3 and Metro Line 4, as shown in Figure 15. The foundation pit is close to Mount Zhai. The terrain is gradually rising from north to south, and groundwater movement is intense. Caves are formed along the fissures and structural surfaces by long-term seepage of surface water in the site. The water pumping test shows that the permeability coefficient is about 3.5 m/d.

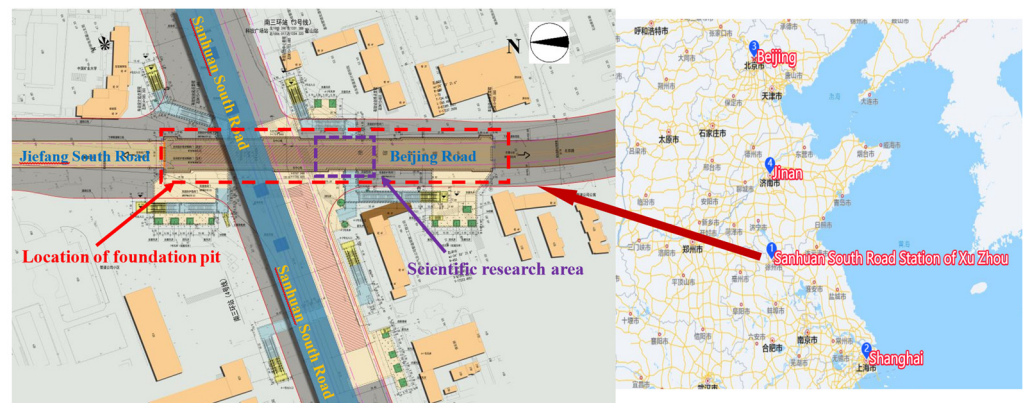


Figure 15. Location diagram of Sanhuan South Road Station.

The foundation pit is excavated to a depth of approximately 30 m, where limestone is mainly developed. The construction method of “cut-bottom up” is adopted for the main foundation pit of the station, and the retaining structure of “retaining pile + horizontal inner supports (anchor cables)” is adopted. A geological section of foundation pit cross section is shown in Figure 16.

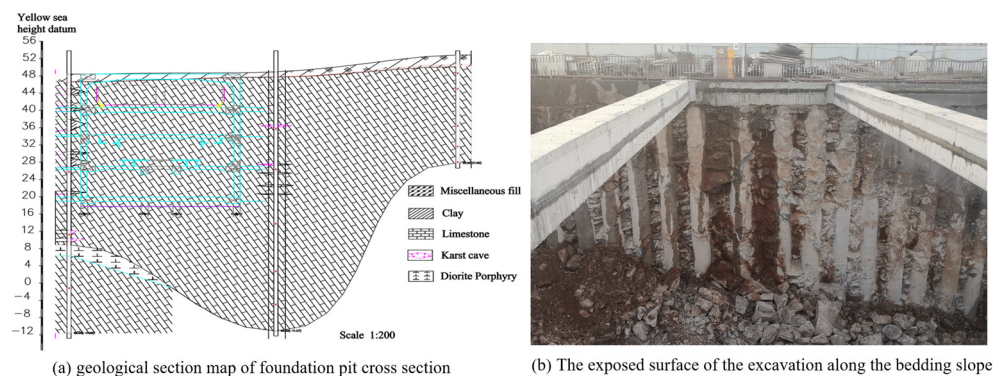


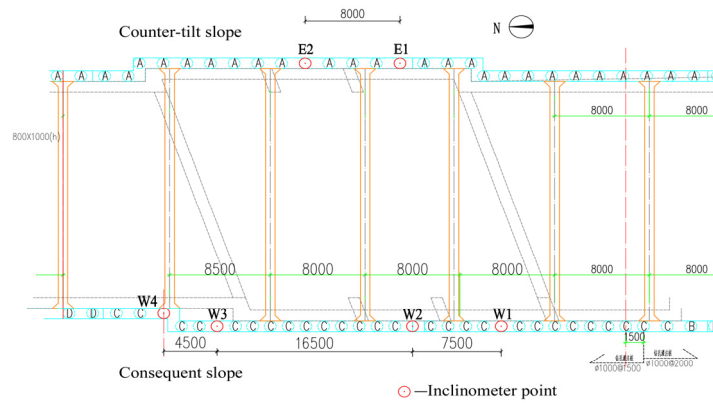
Figure 16. Engineering geological map.

The western side slope of the pit is the bedding rock structural plane (C35 concrete pouring) with a \varnothing 1000 mm @ 1500 mm cast-in situ bored pile (dip angle: 70°). The eastern side slope is the toppling rock structural plane with a \varnothing 1000 mm @ 2000 mm cast-in situ bored pile. Concrete supports (C35 concrete pouring) are used as the first support; steel supports (diameter: 800 mm) are used as the second support; and the third steel support can be set locally. The mechanical parameters of rock mass are shown in Table 3. Structural plane parameters are shown in Table 2.

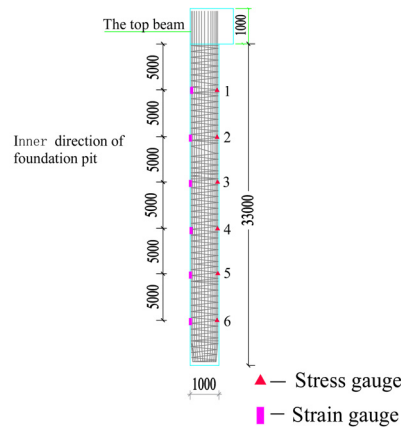
Table 3. Mechanical parameters of the foundation pit slope.

Description	Density (kg/m ³)	Young's Modulus (Pa)	Poisson's Ratio	Cohesion (Pa)	Internal Friction Angle (°)	Compressive Strength (Pa)
Limestone	2680	21.18 × 10 ⁹	0.17	3.0 × 10 ⁶	34	1.0 × 10 ⁶

The slopes of the toppling rock structure plane are monitored by two retaining piles on the east side of the pit under study, while four retaining piles are selected to monitor the slopes of the bedding rock structural plane on the west side, as shown in Figure 17a. Six monitoring points for reinforcement meters are set on the soil-facing side of each retaining pile, and six concrete strainmeters are set on the soil backing side for data calibration, as shown in Figure 17b. Meanwhile, reinforcement meters (soil backing side) and concrete strainmeters (soil facing side) are set on the crown beam, and 13 monitoring points are set correspondingly. A total of seven monitoring points for metal surface strainmeters are set on the steel waist beam, as shown in Figure 17c.



(a)



(b)

Figure 17. Cont.

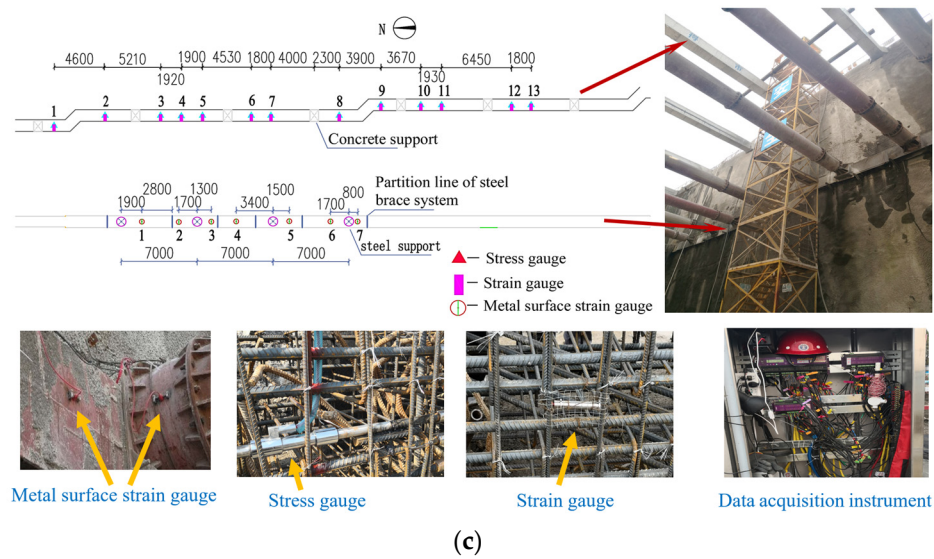


Figure 17. Monitoring point of foundation pit. (a) monitoring point for inclination (unit: mm, scale: 1:200); (b) monitoring points for stress and strain meters of retaining piles (unit: mm, scale: 1:50); (c) monitoring points for stress and strain meters of support beam (unit: mm, scale: 1:200).

Figure 18 shows the horizontal displacement curve of the piles monitored on the bedding rock side and the toppling rock side of the foundation pit, as E1 and W2 were broken during construction and were not analyzed here. The E2 retaining pile is located on the side slopes on the toppling rock side. As seen from Figure 18a, the top of the retaining pile basically slopes toward the interior of the foundation pit until the foundation pit is excavated to $-3F$ (-20 m), which is the same as the trend as the pile displacement curve in Figure 11a. When the foundation pit is excavated to -30 m, the mid- and lower-part of the pile body starts inclining toward the inside of the foundation pit, indicating that the lower rock mass of the foundation pit also starts inclining toward the inside of the foundation pit.

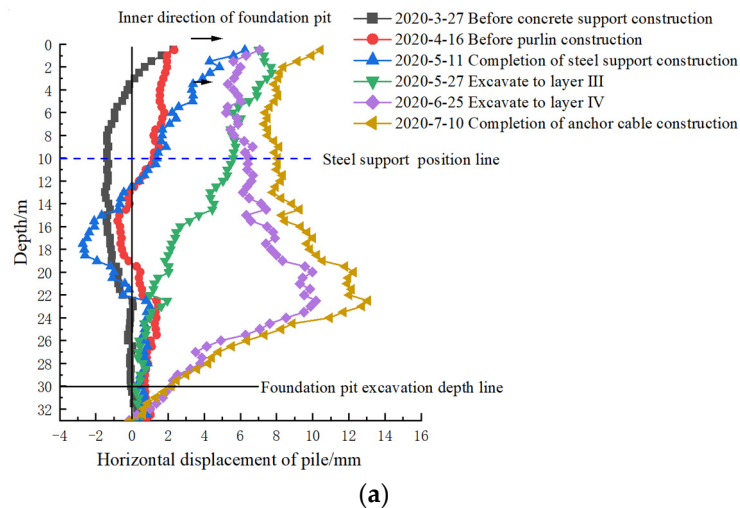


Figure 18. Cont.

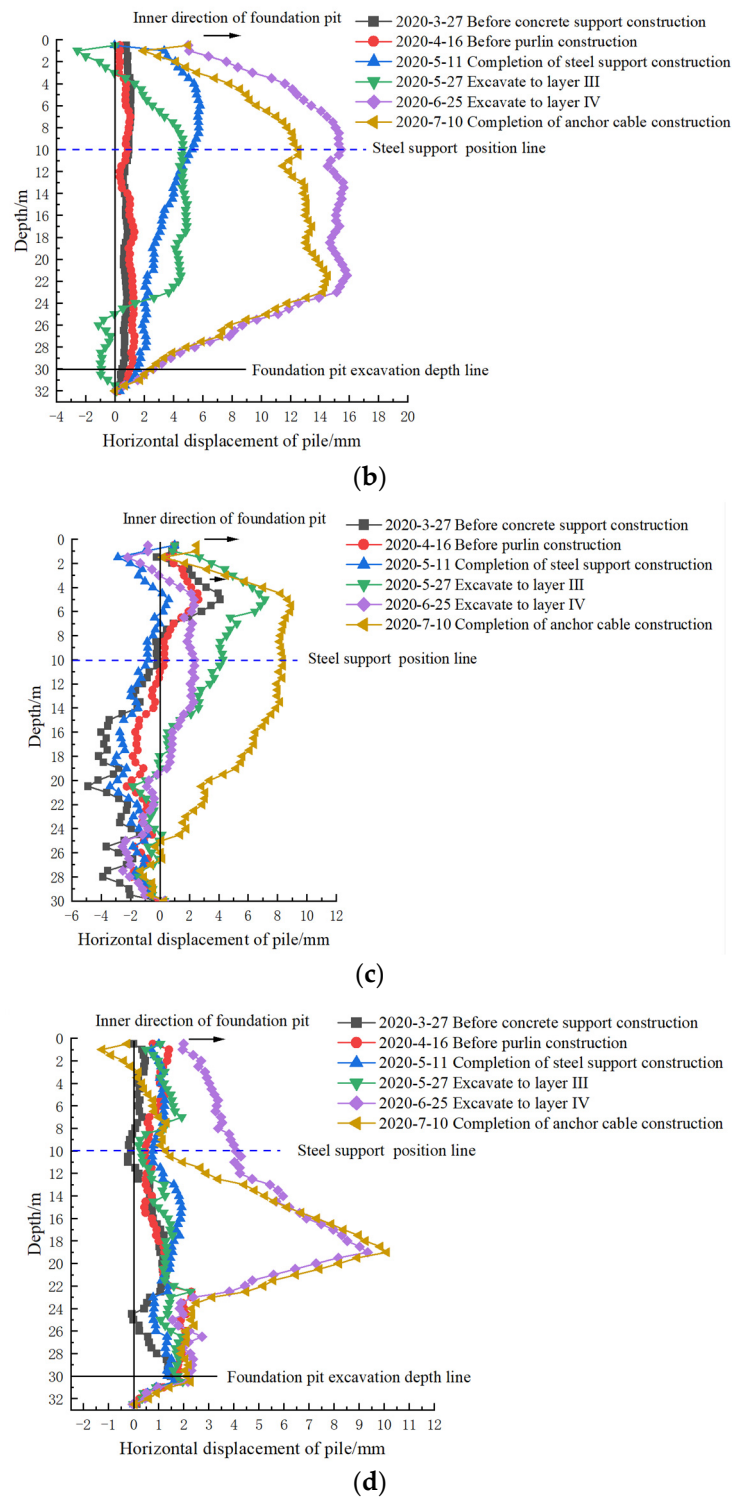


Figure 18. Horizontal displacement curve of retaining pile. (a) E2; (b) W1; (c) W3; (d) W4.

The W1, W3, and W4 retaining piles are located on the side slopes on the bedding rock side in Figure 18b–d. The displacement curve of the W1 pile shows that, as the excavation depth of the pit increases, the salient point of horizontal displacement gradually moves downward with the increase in excavation depth of the foundation pit. Since the third support is set for W1 at -20 m, the maximum displacement occurs between $-10\sim-20$ m when excavation progresses to -30 m.

As the top of the foundation pit at the position corresponding to the W3 retaining pile is located in the stacking area of steel, there is a significant amount of deformation in the front half of the pile under the additional overlying load. Meanwhile, this indicates that the slip surface at the second half of the pile body is not connected with the top surface. Moreover, severe deformation occurred after excavation of W4 to -30 m. In combination with the detection and analysis results of the geological radar, there is a large karst cave at a depth of approximately -15 m, so the structural plane may be connected.

Figure 19a–d shows the change curve of the reinforcement axial force of retaining piles against monitoring duration. The reinforcement meters on the soil facing side basically change from tensile stress to pressure stress during the whole construction period, while the strainmeters show the opposite trend, which is not shown again due to space limitations. According to the deformation curve of the reinforcement meter, the retaining pile deforms from the top under a cantilever state toward the foundation pit at the beginning with the excavation of the foundation pit, gradually being restrained by the support. The middle and lower parts of the pile deform toward the pit and finally become compressed. The entire process corresponds to the measured displacement curve.

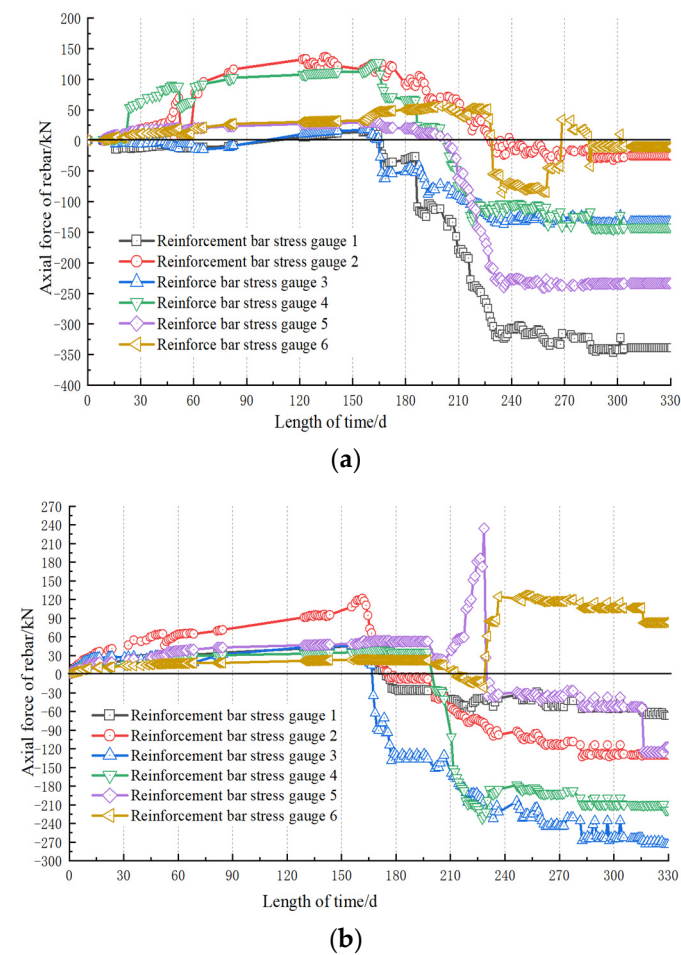
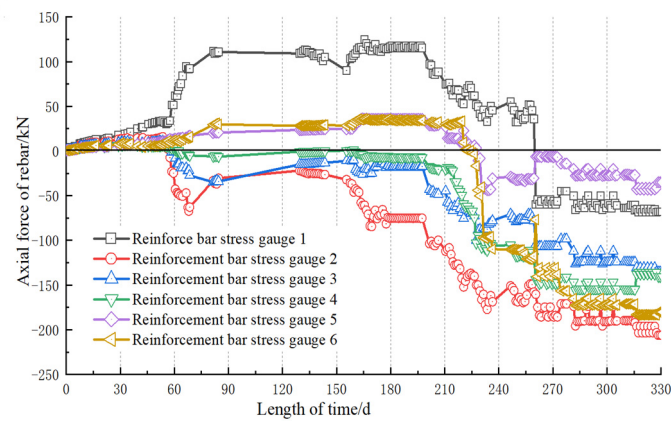
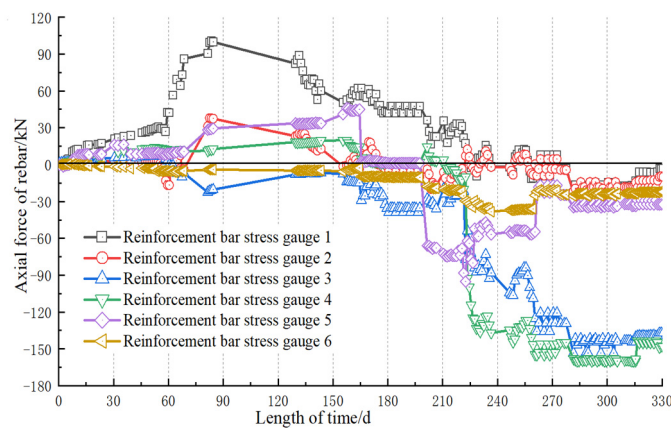


Figure 19. Cont.



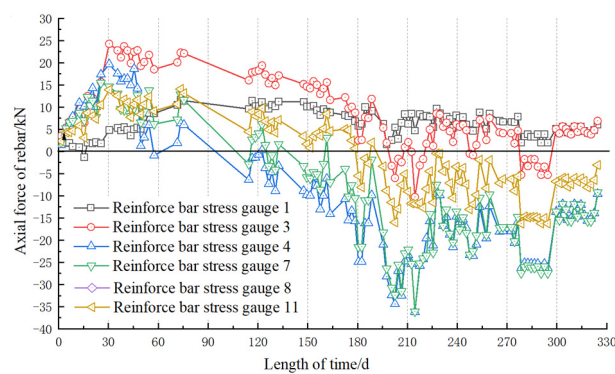
(c)



(d)

Figure 19. Reinforcement axial force curve of retaining piles. (a) E2; (b) W1; (c) W3; (d) W4.

Figures 20 and 21 show the stress change curve of crown beams and the strain change curve of waist beams, respectively. To clearly present the change characteristics of the whole support beam, only some points of the deformation curve are mapped.



(a)

Figure 20. Cont.

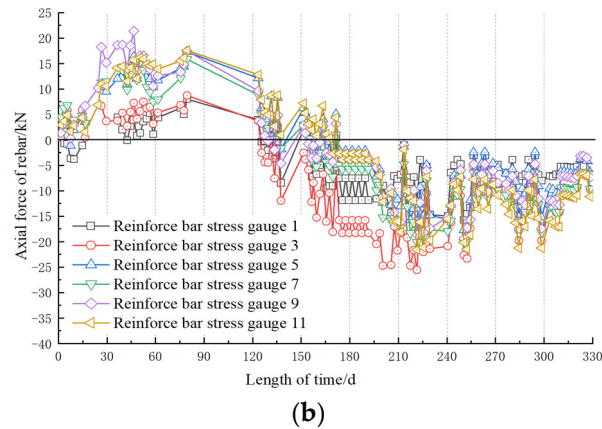


Figure 20. Reinforcement axial force curve of the top beam. (a) side slopes on the toppling rock side; (b) side slopes on the bedding rock side.

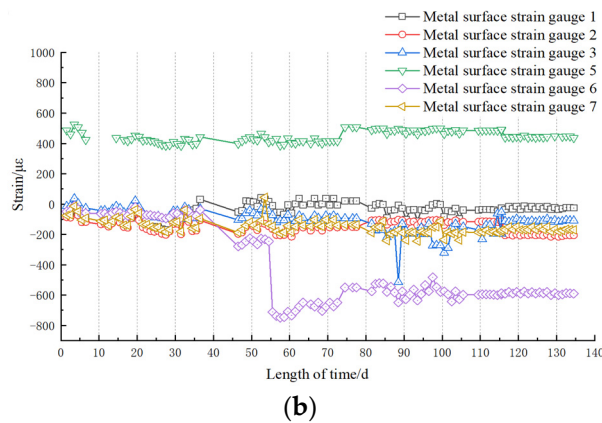
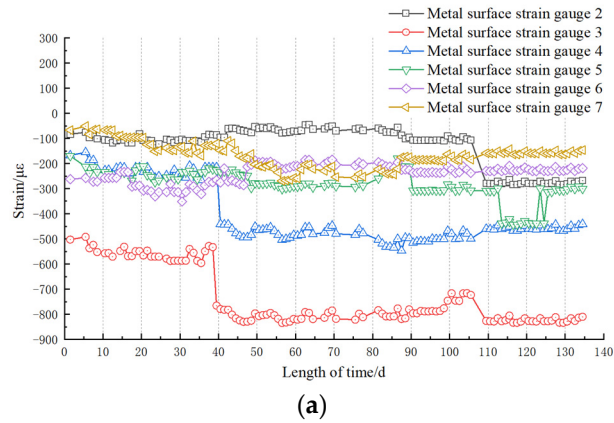


Figure 21. Strain curve of steel waist beam. (a) side slopes on the toppling rock side; (b) side slopes on the bedding rock side.

According to Figure 20a,b, the reinforcement meters of the crown beams on both sides basically show a shift from tensile to stressed, with the maximum stress position located at both ends of the crown beam, where the overall strain of the crown beam on the bedding rock side shows a phenomenon of small in the middle and large on both sides, which is consistent with the displacement curve deformation trend simulated in Figure 12.

The monitored deformation curves for the waist beams are shown in Figure 21a,b. Unlike the simulated situation, steel circuit purlins with a length of approximately 6 m are used for steel waist beams on site, which are not connected to each other as a whole. However, it can also be seen that the strain around the two steel supports in the middle of the toppling rock side is significantly higher than the strains at the other monitoring points

under the effect of steel supports. This indicates an obvious trend of deformation toward the inside of the foundation pit at a depth of -10 m. The strain on the bedding rock side is basically stable (except for some points), indicating no local slip from W1 to W3, which matches the displacement curve.

In order to verify the rationality of the model, the numerical simulation results, the elastic fulcrum method and the measured horizontal displacement calculation results are drawn in Figure 22. In the numerical model, the most disadvantageous situation to select the fracture angle of rock mass is equivalent to an internal friction angle of 62° . Other parameters of rock mass are shown in Table 3. The setting scheme of enclosure piles and selection of the center pile are the same as Figure 11a. It can be seen from Figure 22 that the displacement trends of the three calculation methods are consistent in the bedding rock side of the foundation pit.

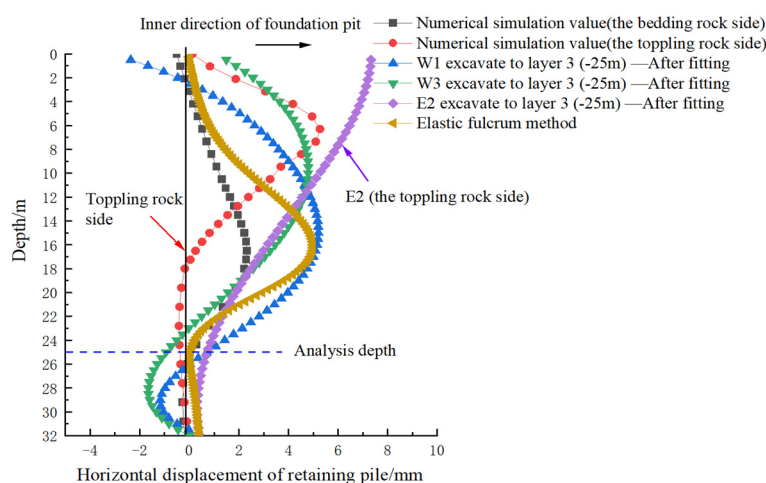


Figure 22. Trend table of horizontal displacement variations for various calculation methods.

In summary, the measured value at monitoring points of the foundation pit may be affected by measuring error and blasting. However, the deformation trend on the bedding rock side is basically identical to that shown by the results of the simulation taking the most unfavorable structural plane inclination; the deformation on the toppling rock side is related to the angle and spacing of the model structural plane, and there is a certain error between the late excavation and the simulation results.

7. Analysis of Optimizing the Foundation Pit Supporting System Based on the Space Effect

It can be identified through the research above that conventional supporting methods have certain disadvantages in controlling the deformation of retaining piles, especially when the slip surface is uncertain. Narrowing the spacing of retaining piles will remarkably increase the supporting cost and construction period, but the greater the excavation depth of foundation pit, the more obvious the space effect [27,28]. Therefore, this paper attempts to adopt the spatial effect-based sectionalized support control technique to artificially construct a dense space to improve the engineering efficiency and support effect, avoiding the influence of weak structure on the overall stability of rock mass [29].

As shown in Figure 23a, the retaining piles on both sides of the reinforcing point are deleted based on the original layout of a pile spacing of 3.0 times, forming the layout mode of “dense in the middle and sparse on both sides”. When a combination of zoning and sparse-dense piles is adopted, the middle piles and side piles on the bedding rock side and the toppling rock side deform almost synchronously, as shown in Figure 23b. This indicates that the remaining sliding force of the entire rock mass is concentrated in the middle of the divided area and that the deleted retaining piles on both sides of the reinforcing point have no influence on the overall supporting effect.

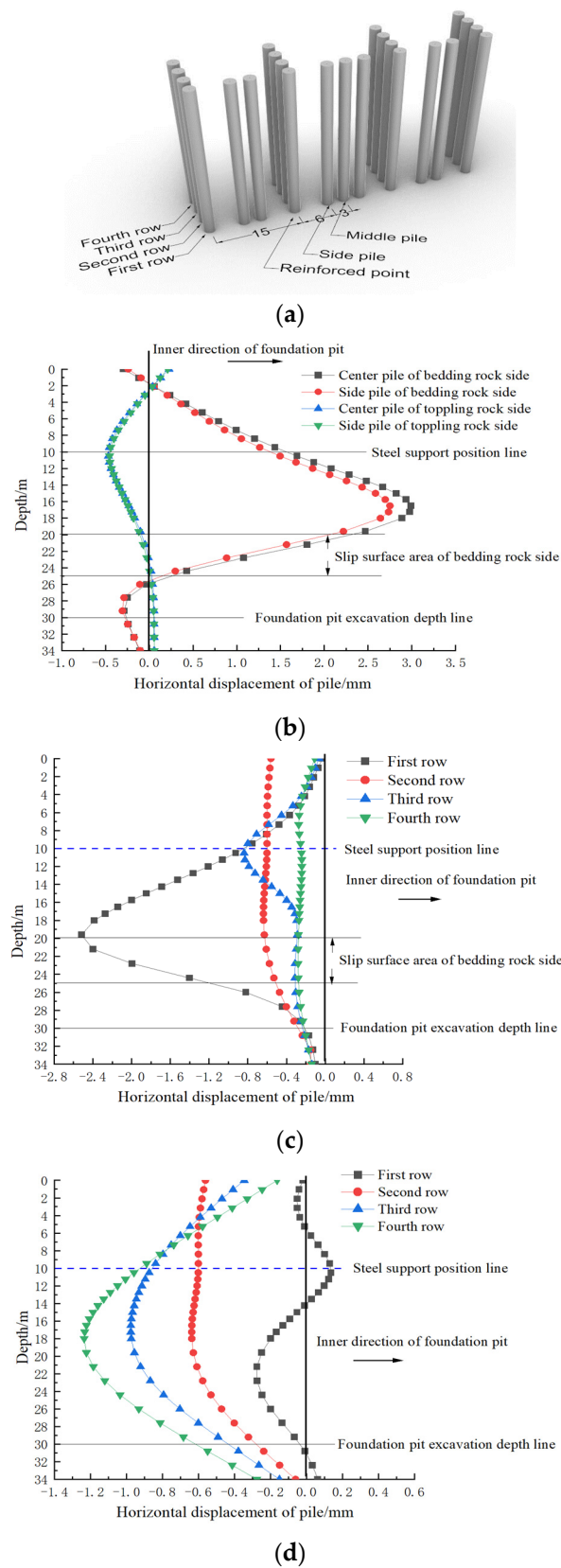


Figure 23. Stress analysis of sectionalized support system (design of sparse-dense pile). (a) schematic diagram of sectionalized sparse-dense pile support model (Unit: m); (b) displacement of retaining pile; (c) displacement of pile body at reinforced point (bedding rock side); (d) displacement of pile body at the reinforced point (toppling rock side).

At the reinforcing point, the tops of the four reinforcement piles were deformed to a large extent, as shown in Figure 23c,d. Specifically, the bedding rock side has the greatest influence on the deformation of the retaining piles in the first row of the reinforcing point, while the toppling rock side has the most pronounced effect on the retaining piles in the fourth row.

To solve the problems of inconsistent deformation and a sharp increase in pile body displacement at the reinforced point, an additional tie beam is considered to be added to the top of the pile top at the reinforced point to form a whole structure with the top beam, thereby restraining the deformation of the retaining pile at the reinforced point and increasing the integrity of the support structure, as shown in Figure 24a.

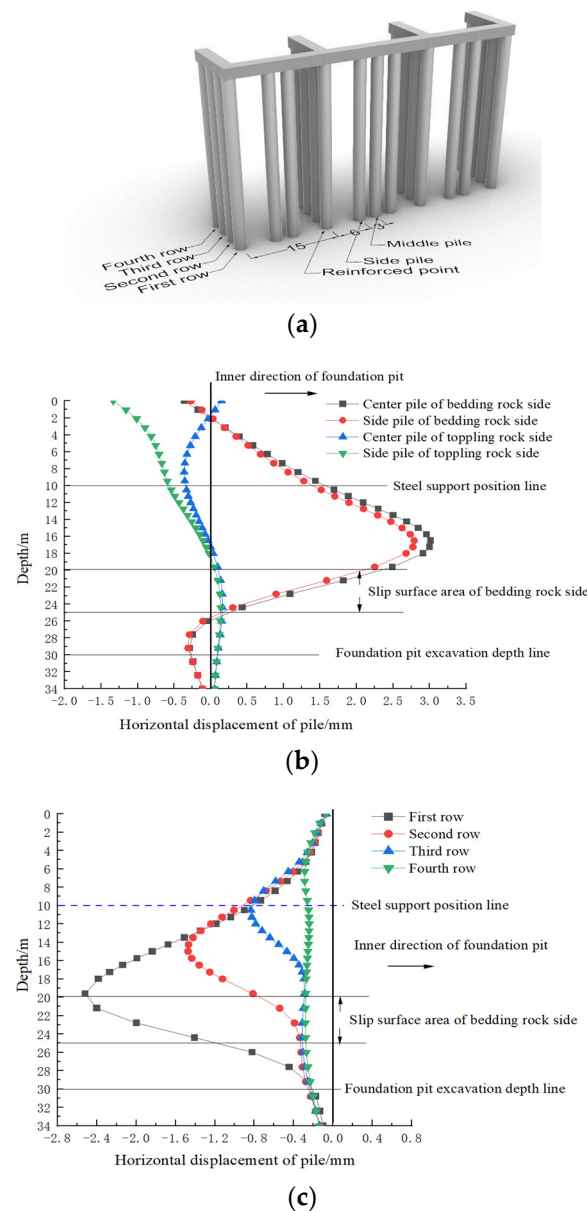


Figure 24. Cont.

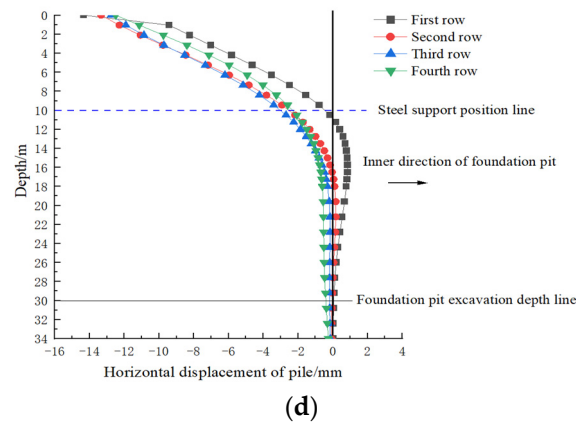


Figure 24. Stress analysis of the sectionalized support system (arrangement of sparse-dense pile and tie-beam). (a) schematic diagram of the support model of sparse-dense pile and tie beam (Unit: m); (b) displacement of retaining pile body; (c) displacement of pile body at reinforced point (bedding rock side); (d) displacement of pile body at the reinforced point (toppling rock side).

It can be seen from the displacement curve of the pile body that the deformation trend of the pile body displacement curve of the middle pile and the side pile on the bedding rock side is synchronized, as shown in Figure 24b, and the maximum deformation of the row pile is the same as when no tie beam is applied.

After the application of the tie beam, the four reinforcement piles on the bedding rock side and on the toppling rock side show the same trend, as shown in Figure 24c,d. The displacement of the pile top of the reinforced pile on the bedding rock side tends to be zero, which shows that the tie beam maintains the consistency of the deformation of the reinforced pile body. Therefore, the application of a tie beam is helpful for the deformation control of retaining piles on bedding rock side slopes. However, since the deformation on the toppling rock side is less than that on the bedding rock side, nonapplication of the tie beam can be considered. Displacement comparison tables of the above support schemes are shown in Table 4.

Table 4. Analysis results of rock slope support.

The Type of Support	The Basic Parameters			Basic Law of Displacement Increase/Decrease after Pile Spacing Change in Bedding Slope (on the Basis of the Previous Level)
	The Pile Diameter (m)	Pile Spacing (Multiple of Pile Diameter)	Longitudinal Length of Model (m)	
Pile-bracing	1.0	1.5, 2.0, 3.0, 4.0	50	1.5 times to 2 times displacement increase by about 12.5%. 2 times to 3 times displacement increase by about 40%. 3 times to 4 times displacement increase by about 18%.
Pile-brace-anchor combination	1.0	4.0	50	Displacement is reduced by about 12% compared to 4.0 times of the pile-bracing structure.
Sectionalized support	1.0	3.0	50	Sparse-dense pile: displacement is reduced by about 14% compared with 3.0 times of pile-bracing. Sparse-dense pile and tie beam: displacement is reduced by 13% compared with 3.0 times of pile-bracing.

8. Conclusions

In this paper, the models of bedding slope and toppling slope of rock slope are established by numerical simulation. On this basis, the deformation characteristics of the traditional row pile supporting scheme are analyzed, and the concept of sectionalized support control is innovatively proposed in view of the limitations of the traditional scheme. The following conclusions could be drawn based on the comprehensive results of the above studies:

- (1) For bedding rock slopes, the failure on the bedding rock side is prone to be affected by karst caves and thus changes the final sliding path to form a broken line landslide, while arc-shaped toppling failure is prone to be formed on the toppling rock side.
- (2) For bedding rock foundation pits, it is recommended to use prestressed anchor cables in conjunction with the anchor cables, which can reduce the maximum displacement by about 12%, while the anchor cable spacing needs to be strictly controlled to maximize the supporting effect of the anchor cables. However, the additional bending load from anchor cables on the pile body on the toppling rock side should be taken into consideration.
- (3) For the foundation pit side slope with a long longitudinal distance, the sectionalized support of the retaining pile could effectively restrict the deformation of the retaining structure and the range of rock landslides. Taking three times the spacing of piles as an example, the maximum displacement of the retaining piles in the bedding direction can be reduced by about 13% under the same spacing of piles.
- (4) On the basis of spatial effect support, the top of the foundation pit on the bedding rock side can be provided with a tie beam for overall reinforcement to maintain the integrity of the support structure. The tie beam can replace the anchor cable, and its support effect can reduce the maximum horizontal displacement by 13% compared with the pile anchor support in the toppling slope.
- (5) For the foundation pit side slope with sectionalized support, if the requirement of final displacement control on the bedding rock side could not be met, prestressed anchor cables could be set above the slip surface, which can further control the deformation of the pile body, while the toppling rock side slope can basically meet the maximum displacement requirements by adopting the sectionalized support design. At the same time, the spacing of piles in the bedding rock side can be extended by 0.5 times as that of the toppling side.
- (6) When using anti-sliding piles to divide the foundation pit section, it is necessary to calculate the stability against sliding of the anti-sliding piles so as to ensure that the integral damage will not occur.
- (7) From the results of monitoring and numerical simulation, the foundation pit of Sanhuan South Road Station is in a safe state. If the traditional pile-anchor support method is adopted, the spacing between piles can be enlarged by three times or the local stability can be improved by using the sectional support method.

Author Contributions: Conceptualization, formal analysis, data curation, and writing, J.X.; supervision, funding acquisition, Y.W. All authors have read and agreed to the published version of the manuscript.

Funding: This work was supported by the National Natural Science Foundation of China (Grant Nos. 52074264 and 51174194) and the National Key Research and Development Program of China (Grant No. 2016YFC0600903).

Institutional Review Board Statement: Not applicable.

Informed Consent Statement: Not applicable.

Data Availability Statement: The data used to support the findings of this study are available from the corresponding author upon request.

Conflicts of Interest: The authors declare no conflict of interest.

References

1. Raghuvanshi, T.K. Plane failure in rock slopes—A review on stability analysis techniques. *J. King Saud Univ. Sci.* **2019**, *31*, 101–109. [[CrossRef](#)]
2. Tang, H.; Yong, R.; Eldin, M.A.M.E. Stability analysis of stratified rock slopes with spatially variable strength parameters: The case of Qianjiangping landslide. *Bull. Eng. Geol. Environ.* **2017**, *76*, 839–853. [[CrossRef](#)]
3. Kamaruzaman, N.; Jamaluddin, T.A. Rock slope stability assessment by using RMRB and SMR methods for future development around Gunung Lang, Ipoh, Perak. *AIP Conf. Proc.* **2016**, *1784*, 060029.
4. Liu, T.; Liu, H. Design and construction of foundation pits in rock area in Qingdao. *Chin. J. Geotech. Eng.* **2010**, *32*, 499–503.
5. Liu, J.; Zhang, D.; Liu, J. Stability analysis of a rock slope and optimized design of its support scheme. *J. Water Resour. Archit. Eng.* **2013**, *11*, 94–98.
6. Bai, X.; Chen, X.; Zhang, M. “Pile—Steel Support—Anchor” System for Foundation in Rock-Soil Layer. *Soil Mech. Found. Eng.* **2019**, *55*, 425–432. [[CrossRef](#)]
7. Liu, X.; Li, B. Analysis of Supporting Analysis of supporting mechanism of micro-steel-pipe piles in rock foundation pit. *Rock Soil Mech.* **2012**, *33*, 217–222.
8. Hou, J.; Tang, Q.; Liu, J. Experimental study on super-deep rock foundation pit under complex environmental condition. *Build. Struct.* **2021**, *51*, 132–137.
9. An, C.; Liang, Y.; Wang, L.; Deng, S.; Sun, Z.; Fan, B.; Zheng, L. Three-dimensional optimization design for the direction angle of anchor cable reinforcement in wedge rock slope. *Rock Soil Mech.* **2020**, *41*, 2765–2772.
10. Zhou, Y.; Wang, X.; Zhu, Y.; Li, J.; Jiang, X. Monitoring and numerical simulation of an interbedding high slope composed of soft and hard strong-weathered rock. *Rock Soil Mech.* **2018**, *39*, 2249–2258.
11. Li, J.; Liu, B.; Wang, Z.; Fan, G. Design and construction of deep foundation pit supporting in rock slope of Chongqing area. *Constr. Technol.* **2008**, *37*, 104–109.
12. Li, J.; Peng, Z.; Li, Y.; Liu, M.F. Application of Bolt-shotcrete Support in Rock Slope Protecting. *Soil Eng. Found.* **2008**, *22*, 30–32.
13. Chen, J.; Tang, H.; Li, X. Some problems on anchor-shotcrete reinforcement application in rock slope. *Earth Sci.* **2001**, *26*, 357–360.
14. Chen, B.; Fan, Q.; Wei, G. Combined Application of Shotcrete-bolt and Pre-anchor Support in Rock Slope Engineering. *Subgrade Eng.* **2006**, *3*, 45–46.
15. Xiao, J.; Zhong, Y.; Zhu, L. Support technology of deep foundation excavation in heavy miscellaneous fill-rock layers. *Constr. Technol.* **2013**, *42*, 59–62.
16. Zhou, T.; Hua, Y. Stability analysis of layered cutting slope soil nailing support structure based on strength reduction method. *Rock Soil Mech.* **2008**, *29*, 417–420.
17. Huang, D.; Ma, H.; Meng, Q.; Song, Y. Study on toppling mechanism and affecting factors of Anti-dip rock slopes with soft-hard interbedded structure. *J. Eng. Geol.* **2021**, *29*, 602–616.
18. Yao, Y.; Zhang, G.; Chen, H.; Wang, M.; Bao, L.; Chang, Z. Study on the failure mechanisms of counter-tilt rock slopes with layered cataclastic structure. *Chin. J. Rock Mech. Eng.* **2021**, *40*, 365–381.
19. Zheng, Y.; Zhao, S.; Deng, W. Numerical simulation on failure mechanism of rock slope by strength reduction FEM. *Chin. J. Rock Mech. Eng.* **2003**, *22*, 1943–1952.
20. Zhang, H.; Zhu, D.; Wang, P.; Wen, H. Analysis of Deformation and Failure Mechanism of Bedding Rock Slope. *Highway* **2021**, *66*, 67–71.
21. Raghuvanshi, T.K.; Ibrahim, J.; Ayalew, D. Slope stability susceptibility evaluation parameter (SSEP) rating scheme—An approach for landslide hazard zonation. *J. Afr. Earth Sci.* **2014**, *99*, 595–612. [[CrossRef](#)]
22. Hamza, T.; Raghuvanshi, T.K. GIS based landslide hazard evaluation and zonation—A case from Jeldu District, Central Ethiopia. *J. King Saud Univ. Sci.* **2017**, *29*, 151–165. [[CrossRef](#)]
23. Ilawe, N.V.; Zimmerman, J.A.; Wong, B.M. Breaking Badly: DFT-D2 gives sizeable errors for tensile strengths in palladium-hydride solids. *J. Chem. Theory Comput.* **2015**, *11*, 5426–5435. [[CrossRef](#)] [[PubMed](#)]
24. Lee, J.H.; Park, J.H.; Soon, A. Assessing the influence of van der Waals corrected exchange-correlation functionals on the anisotropic mechanical properties of coinage metals. *Phys. Rev. B* **2016**, *94*, 024108. [[CrossRef](#)]
25. Abdellah, W.; Abdelhaffez, G.; Saleem, H. Stability assessment of underground openings using different rock support systems. *Rudarsko-geološko-Naftni Zbornik* **2019**, *35*, 49–63.
26. Asker, K.; Fouad, M.T.; Bahr, M.; El-Attar, A. Numerical analysis of reducing tunneling effect on viaduct piles foundation by jet grouted wall. *Min. Miner. Depos.* **2021**, *15*, 75–86. [[CrossRef](#)]
27. Liu, W.; Li, T.; Wan, J. Deformation Characteristic of a Supported Deep Excavation System: A Case Study in Red Sandstone Stratum. *Appl. Sci.* **2022**, *12*, 129. [[CrossRef](#)]
28. Yang, X.H.; Wu, F.W.; Chen, T.; Liu, X. Analysis of Monitoring Results of a Deep Foundation Pit with Pile-Anchor Retaining Structure. *Adv. Civil Ind. Eng. IV* **2014**, *580–583*, 28–33. [[CrossRef](#)]
29. Nehrii, S.; Nehrii, T.; Zolotarova, O.; Volkov, S. Investigation of the geomechanical state of soft adjoining rocks under protective constructions. *Rudarsko-geološko-Naftni Zbornik* **2021**, *36*, 61–71. [[CrossRef](#)]